

Electron-Impact Promoted Selective [2 + 2] Cycloaddition Mediated by Carbon Nanotube. A Variable-Temperature Variable-Voltage Transmission Electron Microscopic Study

Dongxin Liu,[†] Satori Kowashi,[†] Takayuki Nakamuro,[†] Dominik Lungerich,^{†,‡,§} Kaoru Yamanouchi,[†] Koji Harano,^{*,†} Eiichi Nakamura^{*,†}

[†]Department of Chemistry, The University of Tokyo, 7-3-1 Hongo, Bunkyo-ku, Tokyo 113-0033, Japan

[‡]Center for Nanomedicine (CNM), Institute for Basic Science (IBS), IBS Hall, 50 Yonsei-ro, Seodaemun-gu, Seoul, 03722, South Korea.

[§]Graduate Program of Nano Biomedical Engineering (NanoBME), Advanced Science Institute, Yonsei University, Seoul, 03722, South Korea.

ABSTRACT: An electron beam (e-beam) is a particle beam that transfers its kinetic energy via momentum transfer to materials to cause plasmon excitation, electron-impact ionization, and atom displacement, but it lacks the electric dipole transition mechanism for electron excitation of a 0D material. We report herein e-beam-induced [2 + 2] cycloaddition of van der Waals dimers of C₆₀ by the use of 1D carbon nanotubes (CNTs) as a mediator of energy transfer from e-beam to C₆₀. In situ video imaging of individual reaction events with atomic-resolution transmission electron microscopy was the key technology for determination of the pre-exponential factor for the excitation and the activation energy for the ensuing dimerization. We found that the reaction in pristine, oxidized, and damaged CNTs effects three pathways of dimerization via a singlet, triplet, and radical cation, respectively. The overall kinetic profile changed, depending on variations in the kinetic energy of the e-beam (between 60 keV and 120 keV), the nature of the CNTs, and the temperature. The singlet and triplet reactions require approximately 10⁻³ and 10⁻⁶ electrons, respectively, for one reaction event to take place, indicating that the efficiency of the energy transfer from e-beam to C₆₀ via CNT is very low because of the lack of effective mechanism to mediate the energy transfer. We see the chemistry reported here is a rare example of "e-beam catalysis", where CNT under electron irradiation accelerates a chemical reaction that otherwise does not occur. The study indicates the necessity to perform "variable-temperature variable-voltage" kinetic studies in order to properly understand the mechanism of chemical events taking place under e-beam irradiation.

INTRODUCTION

Light is an electromagnetic beam and transfers its energy to a zero-dimensional (0D) material (e.g., π -conjugated molecules) via an electric dipole transition (EDT) mechanism with conservation of spin angular momentum (Figure 1a).¹ The scope of molecular photochemistry and physics has been considerably expanded by the engineering of intersystem crossing (ISC, Figure 1b),² energy transfer (ENT) (Figure 1c),³ charge separation at an electron donor/acceptor interface, etc.^{4,5,6,7,8,9} Being a particle wave, however, a beam of high energy electrons (e-beam) lacks EDT capability, and effects predominantly plasmon excitation, electron-impact ionization (EII), and atom displacement via momentum transfer.¹⁰ It is therefore of great interest for chemists whether one can utilize the kinetic energy of high energy electrons (e.g., 100 keV) to control chemical reactions that requires only several eV. Data has recently accumulated on the interaction of an e-beam with π -electron-rich quasi-1D carbon nanotubes (CNTs), which forms plasmon and, albeit much less efficiently, exciton by electron-impact electron excitation (EIE), as evidenced by electron energy loss spectroscopy.^{11,12} The EIE induced by high energy e-beam occurs with conservation of spin angular momentum.¹³ CNTs resemble 0D materials due to van Hove singularities (Figure 1a),¹⁴ and we therefore envisaged energy transfer from CNT exciton to π -conjugated molecules in an excited CNT (see Figure 2a for [2 + 2] C₆₀

dimerization). We thus analyze the reaction occurring under single-molecule atomic-resolution time-resolved electron microscopic (SMART-EM) under variable temperature and variable acceleration voltage conditions, in the ranges 103–493 K and 60–120 keV, respectively.^{15,16}

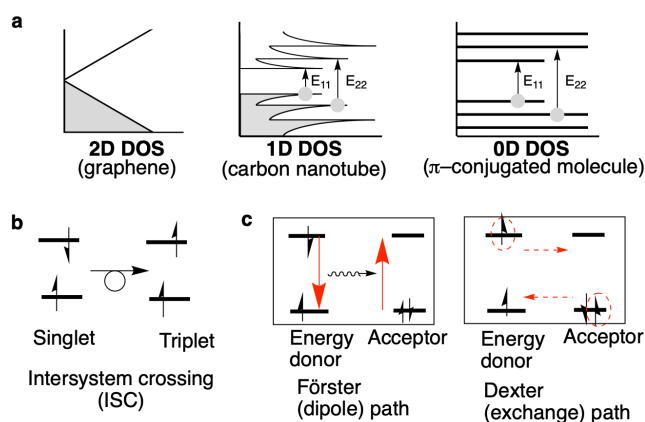


Figure 1. Density of states (DOS) and electron spin interactions. (a) DOS of 0D to 2D materials. (b) Singlet to triplet transition via ISC. (c) Förster and Dexter energy transfer mechanisms.

We report herein that one can choose among pathways of the dimerization of a van der Waals (vdW) dimer of C_{60} in a CNT ($(C_{60})_2@CNT$) by changing the CNT and the kinetic energy of the e-beam (Figure 2a). We identified three pathways of dimerization, a singlet (S_1), triplet (T_1), and radical cation (RC), as characterized by the pre-exponential factor (PEF) of EIE (or EII) and the activation energy (E_a) of the ensuing slow dimerization reactions (Figure 2b). We generated C_{60} in the S_1 state in a pristine CNT (prCNT), the more reactive T_1 species in an oxidized CNT (oxCNT) (Figure 2b), and the highly reactive RC in a damaged CNT (dmCNT) where the π -conjugation was destroyed. The reaction mechanism of the dimerization was found to be highly dependent on the reaction conditions, which hence indicates the risk of making mechanistic interpretations of transmission electron microscopy (TEM) images of chemical events without performing variable-temperature variable-voltage (VT/VV) kinetic analysis. A corollary of this study is that prCNT protects the specimen from radiolysis and charging because of its high-lying filled orbitals (Figure 2c). This observation accounts for the stability of molecules having low-lying HOMOs, such as saturated hydrocarbons,¹⁷ amides,¹⁸ alcohols,¹⁹ and inorganic salts,^{20,21} as observed under single-molecule atomic-resolution time-resolved electron microscopy (SMART-EM) imaging conditions. High stability of organic specimens on conductive indium tin oxide substrates has been documented in scanning electron microscopy (SEM) and has been ascribed to a similar protective effect.²²

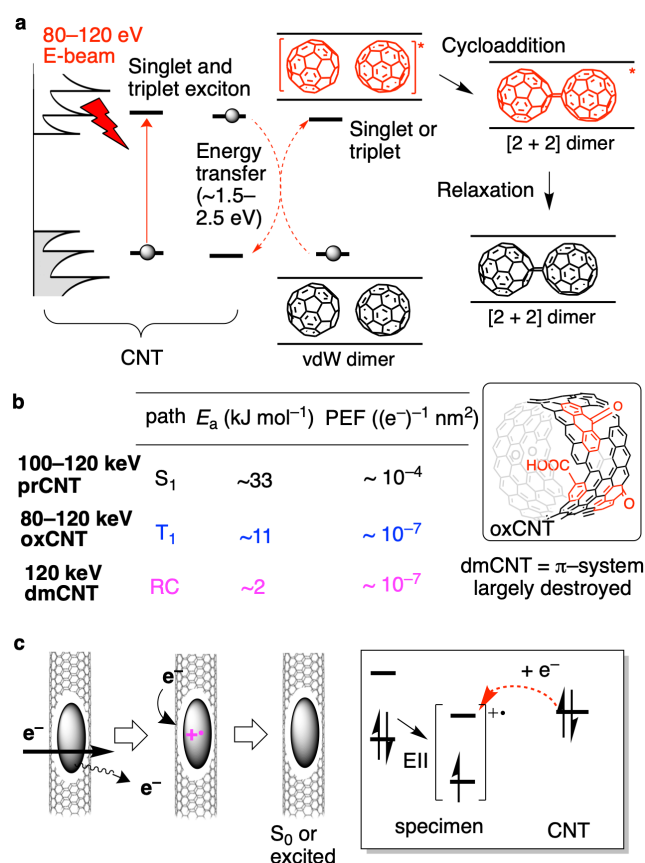


Figure 2. Electron-impact promoted [2 + 2] cycloaddition mediated by CNT-quasi-1D material. (a) [2 + 2] Dimerization of C_{60} by EIE of the CNT followed by ENT from the CNT exciton to C_{60} . The E_{22} transition is shown as a simplified example of transitions responsible for the C_{60} excitation. (b) Representative kinetic parameters of C_{60} dimerization under VT/VV conditions.

(c) Neutralization of an ionized specimen molecule by electron transfer from the prCNT.

RESULTS

The thermally forbidden [2 + 2] dimerization of vdW (C_{60})₂ does not take place at temperatures <800 K.²³ The reaction commences upon photo-irradiation of C_{60} film or solid,^{24,25} also occurs upon electron irradiation (Figure 2a, box). Further irradiation converts the initially formed [2 + 2] dimer eventually to a short CNT²⁶ via retro [2 + 2] cycloaddition and a series of Stone–Wales rearrangements (Figure 3a).²⁷

In 2011, C_{60} dimerization in CNTs was reported to take place even with 20 keV irradiation, although it then requires a 100-times larger electron dose that at 80 keV.²⁸ The 20 keV energy is far lower than the threshold voltage of carbon atom displacement (CAD, knock-on displacement), and the data suggests a mechanism not going through CAD, but through electron impact (EI). A 60-keV electron beam was recently reported to cause reactions of C_{60} sandwiched between two graphene sheets – loss of one carbon atom to form a C_{118} (quasi) dimer via C_{59} .²⁹ This may suggest a difference between a 1D CNT and gapless 2D graphene that lacks van Hove singularities (Figure 1a). This is briefly examined in the present study.

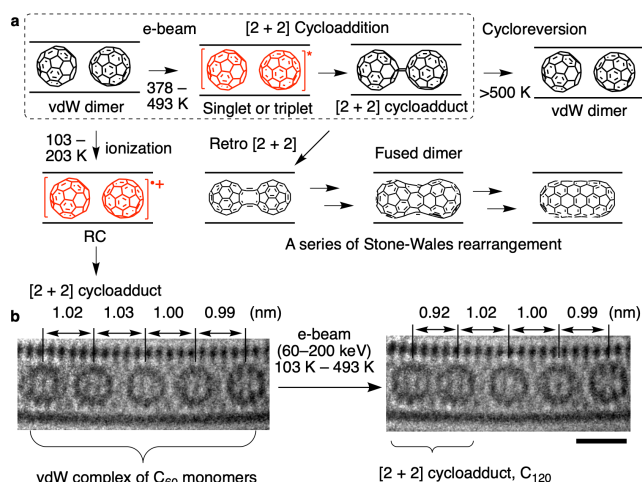


Figure 3. [2 + 2] Cycloaddition via excited state. (a) Cycloaddition via excited state and RC as well as retro cycloaddition and further fusion to produce a short CNT. (b) TEM images of vdW complexes (intermolecular distance 0.99–1.03 Å) and [2 + 2] dimer (0.92 Å). Fused dimer in (a) shows a characteristic intermolecular distance of 0.8 Å. Scale bar = 1 nm.

VT-SMART-EM imaging is an emerging experimental tool for the study of kinetics and thermodynamics of individual chemical events,^{16,19,30} and it has provided direct experimental proof of the Rice–Ramsperger–Kassel–Marcus theory.³¹ In this study, we performed VT-SMART-EM imaging under variable acceleration voltage (VV) conditions (VT/VV-SMART-EM). Following the reaction conditions developed previously,¹⁶ we encapsulated the fullerene molecule in a bundle of pr-, ox-, or dmCNTs, 1.3–1.4 nm in diameter,³² by heating them together at 823 K for 15 h in vacuo. A specimen was deposited on a TEM grid and the time evolution of the [2 + 2] cycloaddition of a (C_{60})₂@CNT was visually monitored with a frame rate of two frames per second (s) under e-beam irradiation at 120, 100, 80,

and 60 kV, with a constant electron dose rate (EDR) of $3.1 \times 10^5 \text{ e}^- \text{ nm}^{-2} \text{ s}^{-1}$ for 120 kV and $5.0 \times 10^6 \text{ e}^- \text{ nm}^{-2} \text{ s}^{-1}$ for 60–100 kV throughout this study. Note that the reaction rate per electron measured in the present work is not affected by the variation of EDR as previously reported.¹⁶

The cycloaddition event was characterized by the change in intermolecular distance from 1.00 nm for the vdW dimer to 0.90 nm for the cycloadduct (Figure 3b), and the E_a and PEF were determined.¹⁶ The [2 + 2] cycloadduct features a strained cyclobutane ring in the middle and reverts to two molecules of C_{60} upon heating at $>500 \text{ K}$, thus providing compelling chemical evidence that the adduct is the C_{120} cycloadduct (Figure 3a).

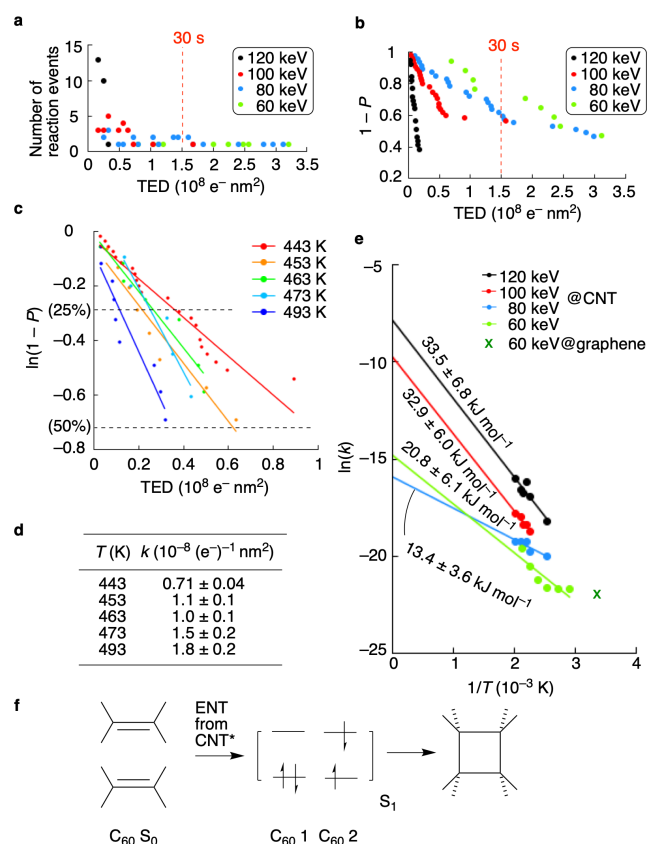


Figure 4. VT/VV-SMART-EM kinetic study of C_{60} dimerization. (a) Occurrence of stochastic reaction events of C_{60} dimerization integrated over every $8.0 \times 10^6 \text{ e}^- \text{ nm}^{-2}$ at 443 K plotted against TED (Table S3, Figure S2). (b) Reaction progress of C_{60} dimerization at 443 K. (c) Semilogarithmic plot of C_{60} dimerization at 100 kV above 443 K and first-order kinetic fitting shown as solid lines. (d) Reaction rate constants of C_{60} dimerization at 100 kV obtained via linear fitting of (c). (e) Arrhenius plot of C_{60} dimerization. The green plot is for the 60-keV reaction, where the slope at higher temperature ($1/T = 2$ to 2.4×10^{-3}) is close to the that of the S_1 path (black, red) and that at lower temperature (2.5 to 3×10^{-3}) is close to the T_1 path (blue). The x indicates the $\ln(k)$ value for dimerization of C_{60} sandwiched between graphene sheets estimated from Figure 4 in ref 29. (f) Mechanistic sketch of the S_1 cycloaddition.

Singlet Dimerization of a $(\text{C}_{60})_2$ @CNT

Unlike light that can transfer its entire energy for electron excitation of molecules via an EDT mechanism, the momentum transfer mechanism available for an electron beam can transfer

its energy to molecules very inefficiently. To assess how inefficient it would be, and to know the consequence of poor efficiency, we performed the kinetic analysis at an acceleration voltage decreasing stepwise from 120 keV to 60 keV.

We first found that a beam of 100–120 keV electrons excites $(\text{C}_{60})_2$ to the S_1 state – a pathway we expect because the EIE with high-energy e-beam occurs with conservation of spin angular momentum.¹³ Rather unexpectedly, however, the S_1 path was unavailable with a beam of 80-keV electron, which instead opened a T_1 path, suggesting that the 80-keV electron generated triplet CNT exciton. ISC from a singlet exciton of CNT to triplet was documented recently.³³ Given the reported S_0/S_1 energy difference of $\sim 2.5 \text{ eV}$ for C_{60} ,³⁴ we estimated that the 100–120 keV e-beam transferred at most $\sim 2.5 \text{ eV}$ to C_{60} , that is, 2 to 2.5×10^{-5} of its kinetic energy ($2.5 \text{ eV}/100\text{--}120 \text{ keV}$). Similarly, the S_0/T_1 energy difference of $\sim 1.5 \text{ eV}$ for C_{60} ³⁴ suggests that at most $\sim 1.9 \times 10^{-5}$ of the 80 keV was utilized for C_{60} excitation.

Taking these numbers into account, we expect that a beam of 60 keV electrons can transfer less than $\sim 1.1 \text{ eV}$ energy to C_{60} via CNT – an energy not enough to excite C_{60} neither to S_1 nor T_1 . We thus reasoned that there would be no dimerization at 60 keV. Nonetheless, the dimerization at 60 keV did place albeit very infrequently. We then reasoned that the reaction took place without CNT excitation; that is, via direct interaction of the 60-keV electron with C_{60} .

In Figure 4, we summarize all the data of the dimerization at 60–120 keV at 443–493 K. The raw data at 443 K are shown in Figure 4a, where we plot the number of dimerization events observed at intervals of $8.0 \times 10^6 \text{ e}^- \text{ nm}^{-2}$ irradiation against the total electron dose (TED) up to $3.0 \times 10^8 \text{ e}^- \text{ nm}^{-2}$ (for 60 s). After in situ monitoring of the reactions of 39–55 C_{60} dimerization events at acceleration voltages of 120 (black), 100 (red), 80 (blue), and 60 kV (green, Figure 4a), we observed three features. First, each reaction event takes place stochastically.³⁵ Second, the occurrence of the events follows the first-order kinetics shown in Figure 4b and c, where the $1-P$ and $\ln(1-P)$ values are plotted against TED (P = normalized conversion of C_{60}). Third, we find three different kinetic profiles.

The rate constants (k) at 100 kV are summarized in Figure 4d. The error is arguably large, for several reasons. The CNT is a mixture of entities having different chirality indexes (i.e., the diameters)³⁶ and, under different physicochemical environments, molecular packing in CNTs changes as the reaction proceeds.

Using the rate constants k obtained at five temperatures, we plotted the Arrhenius plot to obtain the activation energy (E_a , slope) and PEF (y-intercept) (Figure 4e). The E_a values at 120 and 100 kV are nearly identical, 33.5 ± 6.8 and $32.9 \pm 6.0 \text{ kJ mol}^{-1}$, respectively, hence suggesting the same reaction mechanism. The reaction in CNTs under 120 kV ($\text{PEF} = 3.9 \times 10^{-4} (\text{e}^-)^{-1} \text{ nm}^2$) occurs more frequently than the reaction under 100 kV ($\text{PEF} = 5.9 \times 10^{-5} (\text{e}^-)^{-1} \text{ nm}^2$).

The reaction at 80 kV took place with E_a and PEF values essentially the same as those of the T_1 reaction mediated by a triplet-sensitizing oxCNT (see below). We therefore consider the reaction to take place via T_1 . The T_1 species forms less frequently (y-intercept = PEF) but is more reactive than the S_1 species (slope = E_a). An orbital diagram of the concerted singlet cycloaddition is illustrated in Figure 4f.

As discussed above, the reaction at 60 kV was markedly slower at ~ 400 K than the reaction at 100–120 kV (Figure 4b and Figure S3). The Arrhenius plot (green, Figure 4e) deviates from linearity, and we surmise that the kinetics reflects competing S_1 and T_1 , generated by direct EIE and not mediated by the CNT (Figure 2c; see below). Indeed, the estimated E_a value of 20.8 ± 6.1 kJ mol $^{-1}$ and $PEF = 3.7 \times 10^{-7}$ (e $^{-}$) $^{-1}$ nm 2 fall between the values of pure S_1 and pure T_1 .

We estimated the reaction rate of the recently reported dimerization of C_{60} sandwiched between two graphene sheets at 60 kV (Figure 4e caption),²⁹ and obtained $\ln(k) = -21.9$. This data placed at 298 K in Figure 4e (dark green, x) lies close to our 60-kV data, suggesting an electron excitation mechanism.

Triplet Dimerization of a $(C_{60})_2@oxCNT$

The oxCNT (Figure 2b), prepared by $KMnO_4$ oxidation of a CNT,³⁷ has both a π - and σ -carbon skeleton destroyed by chemical oxidation, as evidenced by absorption (due to arene carbonyl groups) in infrared (IR) spectra.³⁸ Therefore, this material may better be viewed as a 0D conjugated material rather than a 1D CNT class of material. It is reported to be a triplet sensitizer in solution, as efficient as benzophenone, and has a triplet energy lower than ~ 2.5 eV.³⁹ We encapsulated C_{60} molecules and conducted VT/VV-SMART-EM experiments with the 30–52 vdW C_{60} dimers in oxCNTs ($(C_{60})_2@oxCNT$) at various temperatures and acceleration voltages.

The raw data of the time course of the dimerization events at 120 kV, with a constant EDR of 3.1×10^5 e $^{-}$ nm $^{-2}$ s $^{-1}$, are shown in Figure 5a, and the frequency integrated over time is shown in Figure 5b. The semilogarithmic plot in Figure 5c gives the reaction rates at 120 kV at temperatures between 378 and 453 K, and the Arrhenius plot gives the E_a and PEF values (Figure 5d). Here, we find that the E_a and PEF agree with values obtained for a prCNT at 80 kV (Figure 4e). A mechanistic sketch of the triplet cycloaddition taking place in two stages via a bi-radical intermediate is illustrated in Figure 5e.

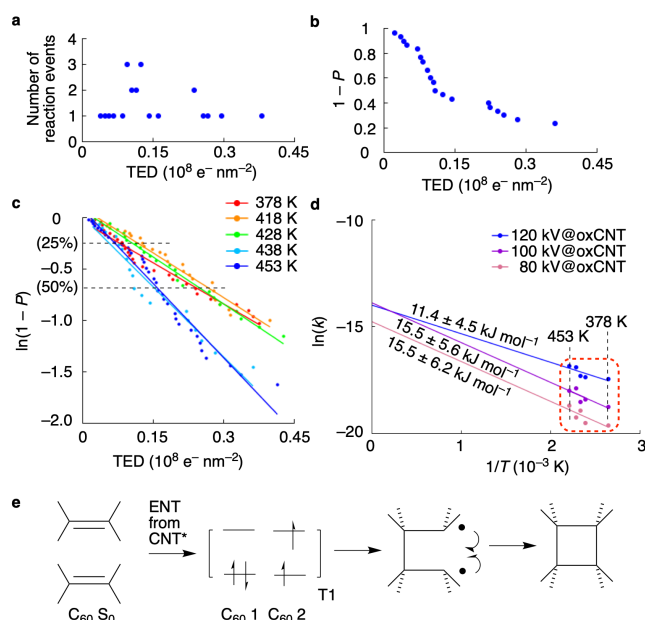


Figure 5. Kinetic study of C_{60} dimerization in an oxCNT. (a) Occurrence of stochastic reaction events of C_{60} dimerization inside oxCNTs at 120 kV integrated over every 8.0×10^6 e $^{-}$ nm $^{-2}$ at 438 K for a $(C_{60})_2@oxCNT$ plotted against TED (Table S4,

Figure S4-5). (b) Reaction progress of C_{60} dimerization inside oxCNTs at 120 kV. (c) First-order kinetics of C_{60} dimerization inside oxCNTs at 120 kV. (d) Arrhenius plot of C_{60} dimerization inside oxCNTs at 80–120 kV. (e) Mechanistic sketch of the T_1 reaction.

It is known that e-beam rapidly destroys the π -conjugation of CNTs at <200 K, as seen in Figure 6a,b,⁴⁰ and that the C_{60} dimerization at 103–203 K exhibits a complex behavior, including the induction period.¹⁶ The reaction had an induction period of variable duration, reflecting destruction of the CNT (Figure 6c). After the induction period, a steady first-order reaction took place. We measured the reaction rate and obtained $E_a = 1.7 \pm 0.6$ kJ mol $^{-1}$ and $PEF = 1.3 \times 10^{-7}$ (e $^{-}$) $^{-1}$ nm 2 (Figure 6d).

The remarkably low E_a value suggests the reactive species to be an extremely reactive RC, formed by ionization. This agrees with the accepted knowledge that ionization is the primary process of destruction of organic molecules by e-beam (radiolysis).⁴¹ A two-step mechanism of the RC reaction is shown in Figure 6e.

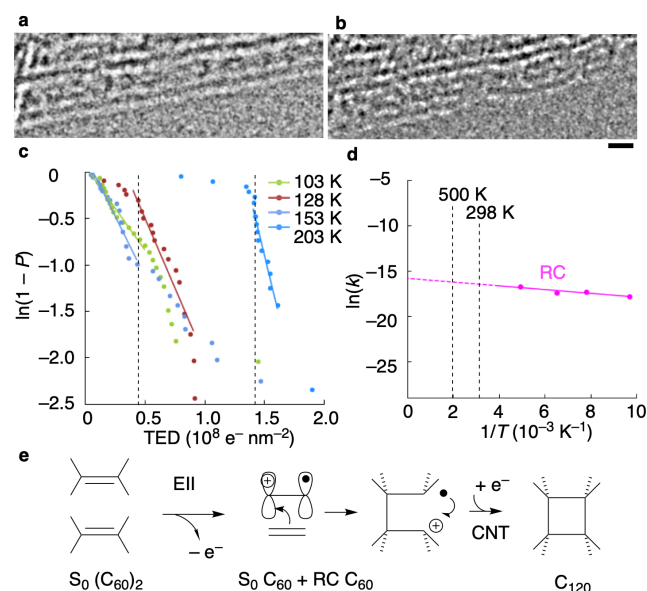


Figure 6. Dimerization at 103–203 K via RC. (a,b) The $C_{60}@prCNT$ decomposes after prolonged irradiation at 153 K to produce $C_{60}@dmCNT$. Scale bar = 1 nm. (c) First-order kinetics of C_{60} dimerization in dmCNTs at 120 kV. Dotted lines show the end of induction period at 128 K and 203 K, from where the rate was calculated. (d) Arrhenius plot of C_{60} dimerization in a dmCNT at 120 kV. (e) Mechanistic sketch of the RC reaction.

We found four types of reactions, as summarized in Table 1 for their representative E_a and PEF data in pr-, ox-, and dmCNTs. The kinetic profiles are color coded in black, blue, green, and purple. The following were recorded at 103–203 K: large E_a (33 kJ mol $^{-1}$) and large PEF ($4\text{--}6 \times 10^{-4}$ (e $^{-}$) $^{-1}$ nm 2 ; black) at 100–120 kV in a prCNT; small E_a (11–15 kJ mol $^{-1}$) and ~ 1000 times smaller PEF ($1\text{--}9 \times 10^{-7}$ (e $^{-}$) $^{-1}$ nm 2 ; blue) at 80–120 kV in an oxCNT (or at 80 kV in prCNT); medium E_a (20.8 kJ mol $^{-1}$) and small PEF (3.7×10^{-7} (e $^{-}$) $^{-1}$ nm 2 ; green) at 60 kV in a prCNT, and nearly zero E_a (1.7 kJ mol $^{-1}$) and the smallest PEF (1.3×10^{-7} (e $^{-}$) $^{-1}$ nm 2 ; purple) in a dmCNT.

We consider that the path with E_a values of $32.9\text{--}33.5 \pm 6 \text{ kJ mol}^{-1}$ in Table 1a (black) took place via S_1 , first because a high-energy e-beam excites CNT with conservation of spin angular momentum, and second because the values compare favorably (within experimental error) with an E_a value of 28 kJ mol^{-1} reported theoretically for S_1 [2 + 2] cycloaddition in gas phase.⁴² We assign the E_a values of $11\text{--}15 \text{ kJ mol}^{-1}$ in Table 1b as obtained for the oxCNT to the T_1 pathway³⁴ because an oxCNT is an effective triplet sensitizer in solution³⁹—a property ascribable to the presence of aromatic ketone residues that accelerate ISC.⁴³ The low values of E_a agree with the biradical character of the T_1 excited state of C_{60} . Similarly, we assign T_1 to the 80-keV experiment in a prCNT (Table 1a) because the kinetic data agree with those for an oxCNT in Table 1b. The value of 20.8 kJ mol^{-1} at 60 keV in Table 1a (green) coincides with a value of 23 kJ mol^{-1} determined for photodimerization possibly accompanying ISC from singlet to triplet.⁴⁴

Table 1. E_a and PEF values obtained from the Arrhenius plot of the C_{60} dimerization events: (a) C_{60} dimerization in a prCNT, (b) in a oxCNT, and (c) in a dmCNT. Color coding according to the reactive species.

a (C_{60})₂@prCNT

e-beam (keV)	E_a (kJ mol ⁻¹)	ln(PEF)	PEF ((e ⁻) ⁻¹ nm ²)	path
120	33.5 ± 6.8	-7.9 ± 1.8	3.9×10^{-4}	S_1
100	32.9 ± 6.0	-9.7 ± 1.6	5.9×10^{-5}	S_1
80	13.4 ± 3.6	-15.9 ± 1.0	1.2×10^{-7}	T_1
60	20.8 ± 6.1	-14.8 ± 1.8	3.7×10^{-7}	S_1/T_1

b (C_{60})₂@oxCNT

e-beam (keV)	E_a (kJ mol ⁻¹)	ln(PEF)	PEF ((e ⁻) ⁻¹ nm ²)	path
120	11.4 ± 4.5	-14.0 ± 1.3	8.3×10^{-7}	T_1
100	15.5 ± 5.6	-13.9 ± 1.9	9.3×10^{-7}	T_1
80	15.5 ± 6.2	-14.8 ± 1.8	3.9×10^{-7}	T_1

c (C_{60})₂@dmCNT

e-beam (keV)	E_a (kJ mol ⁻¹)	ln(PEF)	PEF ((e ⁻) ⁻¹ nm ²)	path
120	1.7 ± 0.6	-15.9 ± 0.5	1.3×10^{-7}	RC

DISCUSSION

The SMART-EM study on the electron-impact promoted [2 + 2] cycloaddition mediated by CNTs (Figure 7) is unique in that we can study in situ the individual reaction events one by one as they take place. The first stage is a fast EIE reaction, characterized by the PEF data. The second stage is a slow thermally driven reaction of excited C_{60} going across an energy barrier with a frequency of $\exp(-E_a/RT)$. We determined the kinetic parameters separately for the two steps by visually monitoring the individual events of the forward cycloaddition of vdW complexes, which excludes the contribution of cycloreversion and reversible collisions from the kinetic data analysis. To our knowledge, this type of information is uniquely available by the VT/VV-SMART-EM technique—it has rarely been obtained in photochemistry research.

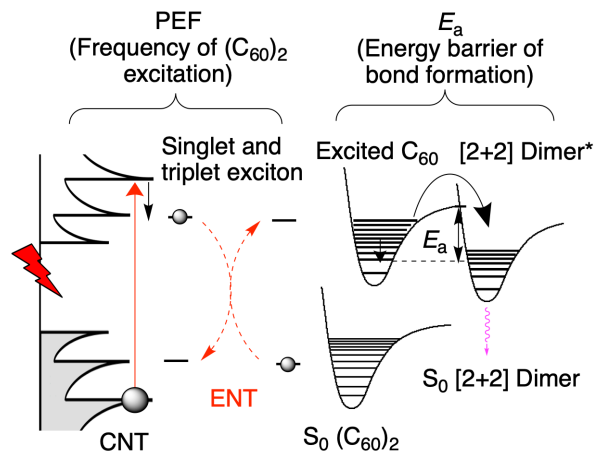


Figure 7. PEF and E_a , representing EIE/ENT and cycloaddition, respectively. Of two possible mechanisms of ENT, the Förster mechanism of ENT is shown. The E_{22} transition is shown as an example of transitions responsible for C_{60} excitation. The E_{33} transition followed by thermal relaxation is shown as an example of the processes involved in the C_{60} excitation.

The ln(PEF) values represent $\ln(k)$ at $T = \infty$, and the large diversity in their magnitude provides an important clue for characterization of the reactive species. These values vary widely, between -7.9 and -16.4 ($\text{PEF} = 3.9 \times 10^{-4} - 1.3 \times 10^{-7} \text{ (e}^{-})^{-1} \text{ nm}^2$). The values are also extremely low, indicating that a large number of electrons ($1.0 \times 10^3 - 3.0 \times 10^6$ electrons) are required to form one excited or ionized C_{60} molecule (area 0.396 nm^2) that produces the dimer. The E_a values (slope) reflect the reactivity of these species in the thermal dimerization reaction (Figure 7, second step).

A parameter that is widely used to evaluate the efficiency of photovoltaic devices is the external quantum efficiency (EQE), which is the ratio of the number of electrons and holes generated by a device to the number of incident photons shining on the device from outside. Similarly, we can define the EQE based on the number of dimers produced to the number of incident electrons, i.e., the ratio of the number of dimerization events to the TED shining on the CNT. The EQE values of the S_1 reaction in a prCNT and the T_1 reaction in an oxCNT at 120 kV are 9.8×10^{-4} and 2.1×10^{-6} , respectively, indicating that the latter is nearly 1000 times less efficient. This is because of the infrequent formation of the triplet exciton of the CNT. The very low value of the energy attenuation factor ($\sim 10^{-5}$; from $\sim 100 \text{ keV}$ to $\sim 2 \text{ eV}$) reflects the lack of a mechanism for efficient energy transfer from the e-beam to CNT and the loss of energy to phonon vibration of CNT and physicochemical processes.

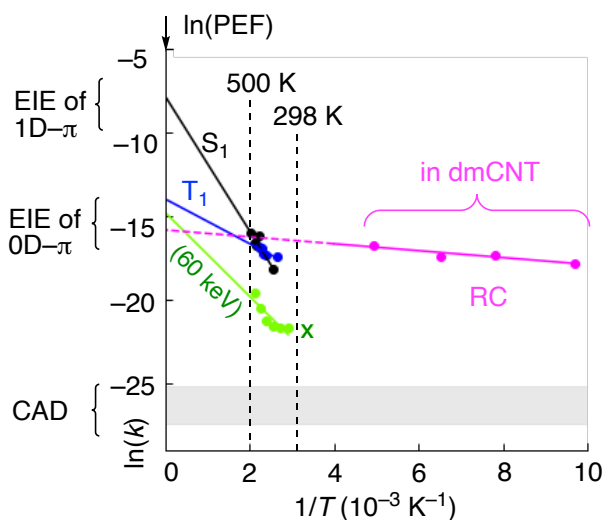


Figure 8. Arrhenius plot for four representative reactions. Black: The 120 kV data in Table 1a via S_1 . Blue: the 120 kV data in Table 1b via T_1 . Green: the 60 kV data in Table 1a via direct EIE. Purple: the 120 kV data in Table 1c via RC. Gray band: a range of $\ln(k)$ values for temperature-independent CAD estimated from $\ln(\text{PEF})$ of radiolysis. The x indicates the $\ln(k)$ value for dimerization of C_{60} sandwiched between graphene sheets estimated from Figure 4 in ref 29.

The Arrhenius plots for the four representative reactions are shown in Figure 8: S_1 in a prCNT (black), T_1 in an oxCNT (blue), RC in a dmCNT (purple), and an electron excited species generated by direct EIE of C_{60} in a prCNT (green). The data reveal the diversity of the reaction mechanism depending on the reaction temperature and CNT that hosts the specimen molecules as well as acceleration voltage.

At 120 keV, the Arrhenius plot is linear at ~ 500 – 400 K and 200 – 100 K, but non-linear at 350 – 200 K (data not shown), suggesting mechanism change because of large difference in E_a among the S_1 , T_1 , and RC reactions. The black line for the C_{60} @prCNT at 120 kV shows the largest $\ln(\text{PEF})$ value of -7.9 , indicating that the reactive species forms most frequently – a behavior expected for an S_1 reactive species.

The other three pathways via EIE or EII occurred ~ 500 times less frequently than the S_1 in the prCNT. Most noticeable is the reaction (purple) that took place with near zero E_a and $\ln(\text{PEF}) = -15.9$, assigned to the reaction of an extremely reactive RC.⁴⁵ We very roughly estimated the $\ln(\text{PEF})$ of CAD of C_{60} to be ~ -25 to -27 , shown as a gray band in Figure 8, on the basis of the $\ln(\text{PEF})$ of RC and the reported frequency difference of $\sim 10^5$ between CAD and radiolysis of polymers.⁴⁶ Since CAD is temperature independent,³⁶ $\ln(k)$ should be ~ -25 to -27 for the temperature range. Thus, the carbon loss of C_{60} would occur approximately $\sim 10^{-5}$ times more slowly than that of the excited state reactions. It should therefore become noticeable only after irradiation with TED of 10^9 – 10^{11} , a dose 100 times greater than the one used for SMART-EM imaging. Note however that the probability of the atom displacement varies as the atomic number varies, changing the cross section of collision and the efficiency of momentum transfer.

In this chemistry of C_{60} dimerization, we can a priori consider four types of reactive intermediates, which differ in their electronic state and number of electrons; neutral (S_0), excited (S_1 or T_1), RC, and radical anion. Out of these, we need to

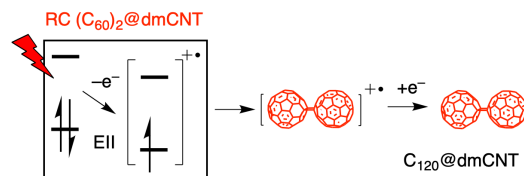
consider the excited and RC, because S_0 is unreactive (thermally forbidden), and high-energy electrons can act as oxidant but not as reductant.

In Figure 9, we schematically illustrate four mechanisms possible in the present system. Chemical reaction triggered by ionization (radiolysis) is the most frequent event seen for organic molecules under TEM conditions,⁴⁶ and hence discussed first. We found it at 103 – 203 K in a dmCNT (a poor electron donor) (Figure 9a-1). Figure 9a-2 illustrates C_{60} ionization taking place in a prCNT (a good electron donor). Here, the CNT donates an electron either to the singly occupied orbital or to a low-lying unoccupied orbital of the RC to generate either S_0 , S_1 or T_1 C_{60} . We consider this to be the process that takes place when a $(C_{60})_2$ @prCNT is irradiated at 60 kV (and perhaps also at 20 kV).²⁸

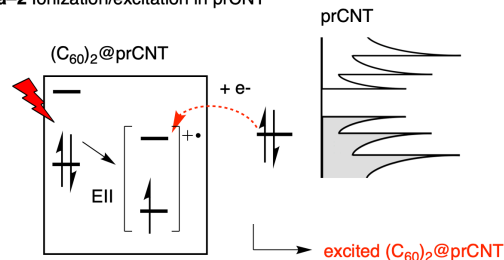
Figure 9b illustrates the S_1 reaction taking place in a prCNT under 100 – 120 kV irradiation. EIE takes place preferentially on quasi-1D CNT rich in delocalized π -electrons, and the CNT exciton transfers energy to C_{60} . Figure 9c illustrates the T_1 pathway for oxCNT. EIE of CNT first generate a singlet exciton, which then undergoes ISC to triplet exciton, and the Dexter-type ENT generates T_1 C_{60} . Note that these reaction mechanisms follow the established reaction mechanisms of electron excitation, energy transfer, and electron transfer except that CNT is a little unusual entity.

a Direct EII of C_{60}

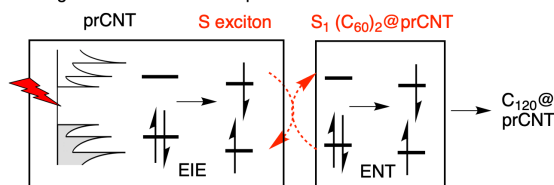
a-1 RC formation/dimerization in dmCNT



a-2 Ionization/excitation in prCNT



b Singlet EIE/Förster ENT in prCNT



c Triplet EIE/Dexter ENT in oxCNT

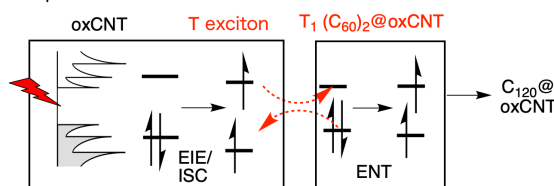


Figure 9. Four pathways available for activation of vdW $(C_{60})_2$ @CNT for $[2 + 2]$ cycloaddition.

CONCLUSION

In summary, we have shown that the excessively large kinetic energy of a high-energy e-beam can be attenuated and utilized for controlling chemical reactions through EIE of CNTs. The reactions show several interesting features. First, the specimen molecule is of unimolecular thickness, and hence secondary electrons play negligible roles. Second, the semiconducting prCNT with its high-lying filled orbital quickly neutralizes any RC that may form by direct EII (Figure 2c), hence protecting the molecule from radiolysis and charging.¹⁵ Similar protective effects of semiconductive substrates such as indium tin oxide have been described in SEM studies.¹⁹

A high-energy e-beam (>80 keV) generates CNT exciton via momentum transfer; it occurs far more frequently on CNTs than on a 0D specimen molecule whose electrons are tightly bound. However, the EQE of the e-beam-induced reactions is extremely low, and only $\sim 10^{-5}$ of the >80-keV e-beam energy is transferred to the molecule via CNTs. Light, on the other hand, can directly transfer its entire energy to a molecule via EDT, and the quantum yield can reach 100%. In this context, we suspect that the e-beam chemistry taking place on zero-gap graphene and metallic substrates show different characteristics (cf. Figure 1a).^{47,48,49,50,51}

Photocatalysis is a technical term to describe the rate acceleration under the action of light irradiation in the presence of a substance that absorbs light (Figure 10a).^{52,53,54} The kinetics of the EIE reactions described above has demonstrated quantitatively the rate acceleration of the [2 + 2] cycloaddition under the action of electron irradiation in the presence of CNTs. We therefore consider the present reaction to be a rare example of e-beam catalysis (Figure 10b). Furthermore, we envisage that SMART-EM technology will be a valuable technology for the exploration of “visual molecular science”.

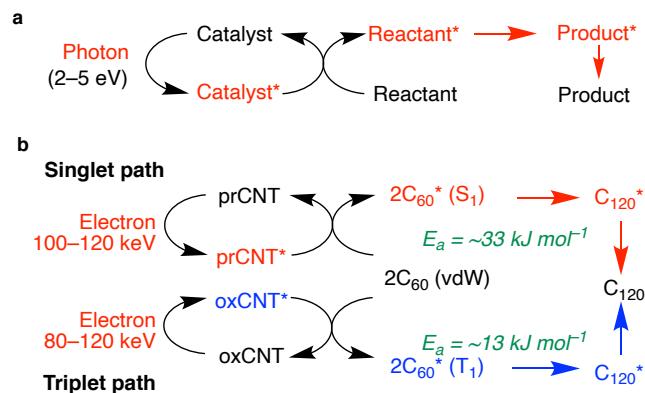


Figure 10. Photocatalysis and e-beam catalysis. (a) Activation of the reactant by photocatalysis. (b) Spin-selective activation of C₆₀ by e-beam catalysis.

EXPERIMENTAL SECTION

Materials Single-walled carbon nanotubes (CNTs, Meijo Arc SO, produced by arc-discharge using Ni and Y catalysts, >99% purity, average diameter 1.4 nm, Lot # 6601316) were purchased from Meijo Nano Carbon Co. Ltd. C₆₀ powder (nanom purple ST, >98% purity) was purchased from Frontier Carbon Corporation. TEM grids precoated with a lacey microgrid (RO-C15, for variable-temperature experiments; pore size 3–8 μm and carbon thickness 70 nm) were purchased from Okenshoji Co., Ltd. Toluene was purchased from Wako Pure Chemical

Industries and purified using a solvent purification system (GlassContour)⁵⁵ equipped with columns of activated alumina and supported copper catalyst (Q-5) prior to use. Potassium permanganate was purchased from Tokyo Chemical Industry Co., Ltd and sulfuric acid was purchased from Wako Pure Chemical Industries.

General The water content of the solvent was determined using a Karl Fischer moisture titrator (CA-21, Mitsubishi) to be <10 ppm. Bath sonication for the dispersion of CNTs in toluene was carried out with a Honda Electronics WT-200-M instrument. Oxidative removal of the terminal caps of CNTs was carried out in an electric furnace ASH ARF-30KC. Encapsulation of C₆₀ into CNTs was carried out in an electric furnace ASH AMF-20, equipped with a temperature controller AMF-9P. IR spectra were recorded on a JASCO FT/IR-6100 instrument with attenuated total reflection. X-ray photoelectron spectroscopy analysis was carried out on a JPS-9010MC instrument using Mg Kα X-rays (1253.6 eV).

Preparation of samples for SMART-EM The C₆₀@CNTs prepared above are in solid form and thus difficult to deposit directly on a TEM microgrid. We therefore first dispersed samples in toluene (0.01 mg/mL), in vials, which were then placed in a bath sonicator for 1 h. The aim was to soften the samples so that we could secure intimate contact between the CNTs and the carbon surface of the grid. A 10 μL solution of the dispersion was then deposited on a TEM grid placed on a paper that absorbs excess toluene. The resulting TEM grid was dried in vacuo (60 Pa) for 2 h.

SMART-EM observation Atomic-resolution TEM observations were carried out on a JEOL JEM-ARM200F instrument equipped with an aberration corrector and cold-field emission gun (point resolution 0.10 nm) at acceleration voltages of $E = 60, 80, 100$, and 120 kV , under $1 \times 10^{-5} \text{ Pa}$ in the specimen column, and with typical spherical aberration values of 1–3 mm. Calibration of the EDR was conducted following a method described in a previous report.¹⁶ C₆₀ dimerization at 60–120 kV and C₆₀ dimerization in oxCNT were monitored at the temperatures mentioned in the main text and an EDR (the number of electrons per second per nm²) of ca. $3.1 \times 10^5 \text{ e}^- \text{ nm}^{-2} \text{ s}^{-1}$ for 120 kV and $5.0 \times 10^6 \text{ e}^- \text{ nm}^{-2} \text{ s}^{-1}$ for 60–100 kV at 800,000× magnification. The imaging instrument was a CMOS camera (Gatan OneView, $4,096 \times 4,096$ pixels), operated in binning 2 mode (output image size $2,048 \times 2,048$ pixels, pixel resolution 0.20 nm at 1,000,000×). A series of TEM images was recorded every 0.5 s as a superposition of 25 consecutive images of 0.04-s frames (automatically processed on Gatan DigitalMicrograph software) over 5–15 min.

We first surveyed C₆₀ encapsulated in CNTs on the screen at 200,000× magnification to identify CNTs for reaction monitoring. Having found bundles of CNTs suitable for kinetic studies, we stopped the beam irradiation and changed the magnification to 800,000×. After waiting for 1 min, until thermal drift of the grid ceased or it was at least relatively relaxed, we commenced observation and movie recording. Focusing was carried out during the collection of images, which was recorded at slightly under-focus conditions (defocus value 10–20 nm). At 80, 100, and 120 kV, we continuously focused on 25–70 molecules in total, with a frame rate of 1.0 s for 5–15 min, until most of the C₆₀ molecules oligomerized to form an inner nanotube. At 60 kV, the recording time was set to be 15–20 min, following the results of kinetic studies at 80 kV.

Temperature control The temperatures were controlled by using a heating holder (JEOL EM-21130). The accuracy of the grid temperature was 2–3 degrees (according to the instrument specifications). After the stage temperature was raised to the setting value, we waited at least 30 min before commencing observations, in order to stabilize the stage for minimization of thermal drift.

Image processing The images were collected as a .dm3 or .dm4 format file on Gatan DigitalMicrograph software and processed using ImageJ 1.47t software for .dm3 files.⁵⁶

Visual data analysis for counting reaction events of C₆₀ dimerization The products of C₆₀ dimerization were visually identified following a protocol described in a previous report,¹⁶ where molecular structures of [2 + 2] cycloadducts were studied thoroughly using atomic-resolution TEM imaging combined with TEM simulations. The progress of the reactions was studied by analyzing the movies backward, from the end of the reaction, to identify C₆₀ dimerization. This procedure eliminates complications due to the intervention of equilibrium caused by thermal cycloreversion. The kinetics of cycloaddition between the fused dimer of C₆₀ molecules and C₆₀ was excluded from the analysis because the resultant product could possess very different properties.

ASSOCIATED CONTENT

- (1) Turro, N. J.; Ramamurthy, V.; Scaiano, J. C. *Principles of Molecular Photochemistry: An Introduction*; University Science Books: 2009.
- (2) Ohmori, N.; Suzuki, T.; Ito, M. Why Does Intersystem Crossing Occur in Isolated Molecules of Benzaldehyde, Acetophenone, and Benzophenone? *J. Phys. Chem.* **1988**, *92*, 1086–1093.
- (3) May, V.; Kühn, O. *Charge and Energy Transfer Dynamics in Molecular Systems*, 3rd revised and enlarged ed.; Wiley-VCH: 2011.
- (4) Kavarnos, G. J. *Fundamentals of Photoinduced Electron Transfer*; Wiley-VCH: 1993.
- (5) Fujishima, A.; Honda, K. Electrochemical Photolysis of Water at a Semiconductor Electrode. *Nature* **1972**, *238*, 37–38.
- (6) Maeda, K.; Teramura, K.; Lu, D.; Takata, T.; Saito, N.; Inoue, Y.; Domen, K. Photocatalyst Releasing Hydrogen from Water. *Nature* **2006**, *440*, 295–295.
- (7) Bergmann, V. W.; Guo, Y.; Tanaka, H.; Hermes, I. M.; Li, D.; Klasen, A.; Bretschneider, S. A.; Nakamura, E.; Berger, R.; Weber, S. A. L. Local Time-Dependent Charging in a Perovskite Solar Cell. *ACS Appl. Mater. Interfaces* **2016**, *8*, 19402–19409.
- (8) Kimura, K.; Miwa, K.; Imada, H.; Imai-Imada, M.; Kawahara, S.; Takeya, J.; Kawai, M.; Galperin, M.; Kim, Y. Selective Triplet Exciton Formation in a Single Molecule. *Nature* **2019**, *570*, 210–213.
- (9) Matsuo, Y.; Sato, Y.; Niinomi, T.; Soga, I.; Tanaka, H.; Nakamura, E. Columnar Structure in Bulk Heterojunction in Solution-Processable Three-Layered p-i-n Organic Photovoltaic Devices Using Tetrabenzoporphyrin Precursor and Silylmethyl[60]Fullerene. *J. Am. Chem. Soc.* **2009**, *131*, 16048–16050.
- (10) Inokuti, M. Inelastic Collisions of Fast Charged Particles with Atoms and Molecules—The Bethe Theory Revisited. *Rev. Mod. Phys.* **1971**, *43*, 297–347.
- (11) Pichler, T.; Knapf, M.; Golden, M. S.; Fink, J.; Rinzler, A.; Smalley, R. E. Localized and Delocalized Electronic States in Single-Wall Carbon Nanotubes. *Phys. Rev. Lett.* **1998**, *80*, 4729–4732.

Supporting Information

The Supporting Information is available free of charge on the ACS Publications website. Experimental procedures, physical properties of the compounds, additional spectra, and characterization data (PDF).

AUTHOR INFORMATION

Corresponding Author

*Correspondence to: harano@chem.s.u-tokyo.ac.jp, nakamura@chem.s.u-tokyo.ac.jp

Notes

The authors declare no competing financial interest.

ACKNOWLEDGMENT

We thank Profs Yuriko Ono, Tetsuya Taketsugu, and Riichiro Saito for fruitful discussions on theoretical aspects of the study. This research is supported by Japan Society for the Promotion of Science (JSPS) KAKENHI (JP19H05459, JP20K15123, and JP21H01758). D. Liu thanks JSPS and the Program of Excellence in Photon Science for a predoctoral fellowship. S.K. thanks MEXT (ALPS program). D. Lungerich thanks JSPS, the Alexander von Humboldt Foundation, and the Institute for Basic Science (IBS-R026-Y1) for financial support.

REFERENCES

- (12) Sato, Y.; Terauchi, M. High-Energy Resolution Electron Energy-Loss Spectroscopy Study of Interband Transitions Characteristic to Single-Walled Carbon Nanotubes. *Microsc. Microanal.* **2014**, *20*, 807–814.
- (13) Allan, M. Study of Triplet States and Short-Lived Negative Ions by Means of Electron Impact Spectroscopy. *J. Electron Spectrosc. Relat. Phenom.* **1989**, *48*, 219–351.
- (14) Carlson, L. J.; Krauss, T. D. Photophysics of Individual Single-Walled Carbon Nanotubes. *Acc. Chem. Res.* **2008**, *41*, 235–243.
- (15) Nakamura, E. Atomic-Resolution Transmission Electron Microscopic Movies for Study of Organic Molecules, Assemblies, and Reactions: The First 10 Years of Development. *Acc. Chem. Res.* **2017**, *50*, 1281–1292.
- (16) Okada, S.; Kowashi, S.; Schweighauser, L.; Yamanouchi, K.; Harano, K.; Nakamura, E. Direct Microscopic Analysis of Individual C₆₀ Dimerization Events: Kinetics and Mechanisms. *J. Am. Chem. Soc.* **2017**, *139*, 18281–18287.
- (17) Koshino, M.; Tanaka, T.; Solin, N.; Suenaga, K.; Isobe, H.; Nakamura, E. Imaging of Single Organic Molecules in Motion. *Science* **2007**, *316*, 853–853.
- (18) Nakamura, E.; Koshino, M.; Tanaka, T.; Niimi, Y.; Harano, K.; Nakamura, Y.; Isobe, H. Imaging of Conformational Changes of Biotinylated Triamide Molecules Covalently Bonded to a Carbon Nanotube Surface. *J. Am. Chem. Soc.* **2008**, *130*, 7808–7809.
- (19) Hanayama, H.; Yamada, J.; Tomotsuka, I.; Harano, K.; Nakamura, E. Rim Binding of Cyclodextrins in Size-Sensitive Guest Recognition. *J. Am. Chem. Soc.* **2021**, *143*, 5786–5792.
- (20) Xing, J.; Schweighauser, L.; Okada, S.; Harano, K.; Nakamura, E. Atomistic Structures and Dynamics of Prenucleation Clusters in MOF-2 and MOF-5 Syntheses. *Nat. Commun.* **2019**, *10*, 3608.
- (21) Nakamuro, T.; Sakakibara, M.; Nada, H.; Harano, K.; Nakamura, E. Capturing the Moment of Emergence of Crystal Nucleus from Disorder. *J. Am. Chem. Soc.* **2021**, *143*, 1763–1767.
- (22) Harano, K.; Minami, K.; Noiri, E.; Okamoto, K.; Nakamura, E. Protein-Coated Nanocapsules via Multilevel Surface Modification. Controlled Preparation and Microscopic

- Analysis at Nanometer Resolution. *Chem. Commun.* **2013**, 49, 3525–3527.
- (23) Bandow, S.; Takizawa, M.; Hirahara, K.; Yudasaka, M.; Iijima, S. Raman Scattering Study of Double-Wall Carbon Nanotubes Derived from the Chains of Fullerenes in Single-Wall Carbon Nanotubes. *Chem. Phys. Lett.* **2001**, 337, 48–54.
- (24) Rao, A. M.; Zhou, P.; Wang, K.-A.; Hager, G. T.; Holden, J. M.; Wang, Y.; Lee, W.-T.; Bi, X.-X.; Eklund, P. C.; Cornett, D. S.; Duncan, M. A.; Amster, I. J. Photoinduced Polymerization of Solid C₆₀ Films. *Science* **1993**, 259, 955–957.
- (25) Wang, Y.; Holden, J. M.; Dong, Z.-H.; Bi, X.-X.; Eklund, P. C. Photo-Dimerization Kinetics in Solid C₆₀ Films. *Chem. Phys. Lett.* **1993**, 211, 341–345.
- (26) Koshino, M.; Niimi, Y.; Nakamura, E.; Kataura, H.; Okazaki, T.; Suenaga, K.; Iijima, S. Analysis of the Reactivity and Selectivity of Fullerene Dimerization Reactions at the Atomic Level. *Nat. Chem.* **2010**, 2, 117–124.
- (27) Han, S.; Yoon, M.; Berber, S.; Park, N.; Osawa, E.; Ihm, J.; Tománek, D. Microscopic Mechanism of Fullerene Fusion. *Phys. Rev. B* **2004**, 70, 113402.
- (28) Kaiser, U.; Biskupek, J.; Meyer, J. C.; Leschner, J.; Lechner, L.; Rose, H.; Stöger-Pollach, M.; Khlobystov, A. N.; Hartel, P.; Müller, H.; Haider, M.; Eyhusen, S.; Benner, G. Transmission Electron Microscopy at 20 KV for Imaging and Spectroscopy. *Ultramicroscopy* **2011**, 111, 1239–1246.
- (29) Mirzayev, R.; Mustonen, K.; Monazam, M. R. A.; Mittelberger, A.; Pennycook, T. J.; Mangler, C.; Susi, T.; Kotakoski, J.; Meyer, J. C. Buckyball Sandwiches. *Sci. Adv.* **2017**, 3, e1700176.
- (30) Jordan, J. W.; Fung, K. L. Y.; Skowron, S. T.; Allen, C. S.; Biskupek, J.; Newton, G. N.; Kaiser, U.; Khlobystov, A. N. Single-Molecule Imaging and Kinetic Analysis of Intermolecular Polyoxometalate Reactions. *Chem. Sci.* **2021**, 12, 7377–7387.
- (31) Laidler, K. J. Elementary Gas-Phase Reactions. In *Chemical Kinetics*, 3rd ed.; Prentice Hall: 1987.
- (32) Shimizu, T.; Lungerich, D.; Stuckner, J.; Murayama, M.; Harano, K.; Nakamura, E. Real-Time Video Imaging of Mechanical Motions of a Single Molecular Shuttle with Sub-Millisecond Sub-Angstrom Precision. *Bull. Chem. Soc. Jpn.* **2020**, 93, 1079–1085.
- (33) Palotás, J.; Negyedi, M.; Kollarics, S.; Bojtór, A.; Rohringer, P.; Pichler, T.; Simon, F. Incidence of Quantum Confinement on Dark Triplet Excitons in Carbon Nanotubes. *ACS Nano* **2020**, 14, 11254–11261.
- (34) Fraelich, M. R.; Weisman, R. B. Triplet States of Fullerene C₆₀ and C₇₀ in Solution: Long Intrinsic Lifetimes and Energy Pooling. *J. Phys. Chem.* **1993**, 97, 11145–11147.
- (35) Bunker, D. L.; Hase, W. L. On non-RRKM unimolecular kinetics: Molecules in general, and CH₃NC in particular. *J. Chem. Phys.* **1973**, 59, 4621–4632.
- (36) Yomogida, Y.; Tanaka, T.; Zhang, M.; Yudasaka, M.; Wei, X.; Kataura, H. Industrial-Scale Separation of High-Purity Single-Chirality Single-Wall Carbon Nanotubes for Biological Imaging. *Nat. Commun.* **2016**, 7, 12056.
- (37) Wepasnick, K. A.; Smith, B. A.; Schrote, K. E.; Wilson, H. K.; Diegelmann, S. R.; Fairbrother, D. H. Surface and Structural Characterization of Multi-Walled Carbon Nanotubes Following Different Oxidative Treatments. *Carbon* **2011**, 49, 24–36.
- (38) Kim, U. J.; Furtado, C. A.; Liu, X.; Chen, G.; Eklund, P. C. Raman and IR Spectroscopy of Chemically Processed Single-Walled Carbon Nanotubes. *J. Am. Chem. Soc.* **2005**, 127, 15437–15445.
- (39) Chen, C.-Y.; Zepp, R. G. Probing Photosensitization by Functionalized Carbon Nanotubes. *Environ. Sci. Technol.* **2015**, 49, 13835–13843.
- (40) Urita, K.; Suenaga, K.; Sugai, T.; Shinohara, H.; Iijima, S. In Situ Observation of Thermal Relaxation of Interstitial-Vacancy Pair Defects in a Graphite Gap. *Phys. Rev. Lett.* **2005**, 94, 155502.
- (41) Egerton, R. F. Radiation Damage to Organic and Inorganic Specimens in the TEM. *Micron* **2019**, 119, 72–87.
- (42) Zobač, V.; Lewis, J. P.; Abad, E.; Mendieta-Moreno, J. I.; Hapala, P.; Jelinek, P.; Ortega, J. Photo-Induced Reactions from Efficient Molecular Dynamics with Electronic Transitions Using the FIREBALL Local-Orbital Density Functional Theory Formalism. *J. Phys.: Condens. Matter* **2015**, 27, 175002.
- (43) Yu, H.; Jin, Y.; Peng, F.; Wang, H.; Yang, J. Kinetically Controlled Side-Wall Functionalization of Carbon Nanotubes by Nitric Acid Oxidation. *J. Phys. Chem. C* **2008**, 112, 6758–6763.
- (44) Sakai, M.; Ichida, M.; Nakamura, A. Raman Scattering Study of Photopolymerization Kinetics in C₆₀ Crystals. *Chem. Phys. Lett.* **2001**, 335, 559–566.
- (45) Hashiguchi, M.; Inada, H.; Matsuo, Y. Solution-Phase Synthesis of Dumbbell-Shaped C₁₂₀ by FeCl₃-Mediated Dimerization of C₆₀. *Carbon* **2013**, 61, 418–422.
- (46) Egerton, R. F.; Takeuchi, M. Radiation Damage to Fullerite (C₆₀) in the Transmission Electron Microscope. *Appl. Phys. Lett.* **1999**, 75, 1884–1886.
- (47) Markevich, A.; Kurasch, S.; Lehtinen, O.; Reimer, O.; Feng, X.; Müllen, K.; Turchanin, A.; Khlobystov, A. N.; Kaiser, U.; Besley, E. Electron Beam Controlled Covalent Attachment of Small Organic Molecules to Graphene. *Nanoscale* **2016**, 8, 2711–2719.
- (48) Russo, C. J.; Passmore, L. A. Ultrastable Gold Substrates for Electron Cryomicroscopy. *Science* **2014**, 346, 1377–1380.
- (49) Naydenova, K.; Peet, M. J.; Russo, C. J. Multifunctional Graphene Supports for Electron Cryomicroscopy. *Proc. Natl. Acad. Sci.* **2019**, 116, 11718–11724.
- (50) Lungerich, D.; Hoelzel, H.; Harano, K.; Jux, N.; Amsharov, K. Yu.; Nakamura, E. A Singular Molecule-to-Molecule Transformation on Video: The Bottom-Up Synthesis of Fullerene C₆₀ from Truxene Derivative C₆₀H₃₀. *ACS Nano* **2021**, 15, 12804–12814.
- (51) Susi, T.; Meyer, J. C.; Kotakoski, J. Quantifying Transmission Electron Microscopy Irradiation Effects Using Two-Dimensional Materials. *Nat. Rev. Phys.* **2019**, 1, 397–405.
- (52) IUPAC. Compendium of Chemical Terminology, 2nd ed. (the "Gold Book"). Compiled by A. D. McNaught and A. Wilkinson. Blackwell Scientific Publications, Oxford (1997). Online version (2019-) created by S. J. Chalk. ISBN 0-9678550-9-8.
- (53) Melchionna, M.; Fornasiero, P. Updates on the Roadmap for Photocatalysis. *ACS Catal.* **2020**, 10, 5493–5501.
- (54) Li, X.; Yu, J.; Wageh, S.; Al-Ghamdi, A. A.; Xie, J. Graphene in Photocatalysis: A Review. *Small* **2016**, 12, 6640–6696.
- (55) Pangborn, A. B.; Giardello, M. A.; Grubbs, R. H.; Rosen, R. K.; Timmers, F. J. Safe and Convenient Procedure for Solvent Purification. *Organometallics* **1996**, 15, 1518–1520.
- (56) Schneider, C. A.; Rasband, W. S.; Eliceiri, K. W. NIH Image to ImageJ: 25 Years of Image Analysis. *Nat. Methods* **2012**, 9, 671–675.

E-beam catalysis in [2 + 2] cycloaddition

